Single-crystal growth and study of the mixed spin-dimer system $Ba_{3-x}Sr_xCr_2O_8$

Alsu Gazizulina,[1] Diana L. Quintero-Castro,[2,3] and Andreas Schilling[1]
[1]*Physik-Institut, Universität Zürich, Winterthurerstrasse 190, CH-8057 Zürich, Switzerland*
[2]*Helmholtz Zentrum Berlin für Materialien und Energie, D-14109 Berlin, Germany*
[3]*Department of Mathematics and Natural Sciences, University of Stavanger, N-4036 Stavanger, Norway*
(Received 10 July 2017; revised manuscript received 5 October 2017; published 7 November 2017)

The compounds $Sr_3Cr_2O_8$ and $Ba_3Cr_2O_8$ are insulating dimerized antiferromagnets with Cr^{5+} magnetic ions. These spin-$\frac{1}{2}$ ions form hexagonal bilayers with a strong intradimer antiferromagnetic interaction that leads to a singlet ground state and gapped triplet states. We report on the effect on the magnetic properties of $Sr_3Cr_2O_8$ by introducing chemical disorder upon replacing Sr by Ba. Two single crystals of $Ba_{3-x}Sr_xCr_2O_8$ with $x = 2.9$ (3.33% of *mixing*) and $x = 2.8$ (6.66% of *mixing*) were grown in a four-mirror-type optical floating-zone furnace. The magnetic properties of these compounds were studied by magnetization measurements. Inelastic neutron-scattering measurements on $Ba_{0.1}Sr_{2.9}Cr_2O_8$ were performed in order to determine the interaction constants and the spin gap for $x = 2.9$. The intradimer interaction constant is found to be $J_0 = 5.332(2)$ meV, about 4% smaller than that of pure $Sr_3Cr_2O_8$, whereas the interdimer exchange interaction J_e is smaller by 7%. These results indicate a noticeable change in the magnetic properties by a random substitution effect.

DOI: 10.1103/PhysRevB.96.184201

I. INTRODUCTION

Quantum magnetism is one of the most active areas of research in condensed-matter physics. One of the reasons to study certain gapped quantum systems is the phenomenon of *equilibrium* Bose-Einstein condensation (BEC) of magnetic quasiparticles, which is one of the most fascinating phenomena predicted by quantum mechanics [1]. The introduction of impurities in such systems has become an important topic since their discovery because quantum disordered spin systems behave differently from classical ones. Despite the difficulty in dealing with local quantum fluctuations, many important results have already been obtained in quantum disordered systems (see, e.g., Ref. [2] for a review).

In the isostructural antiferromagnetic $Ba_3Cr_2O_8$ and $Sr_3Cr_2O_8$ spin-dimer systems, the magnetic ions with a single electron in the $3d$ shell ($s = \frac{1}{2}$) are located in an oxygen tetrahedron. The dominant antiferromagnetic exchange coupling J_0 between pairs of Cr^{5+} ions creates spin dimers which are in a nonmagnetic singlet state in a zero external magnetic field. By applying an external magnetic field larger than a critical value, so-called triplons can form in the network of dimers, which can be considered as a direct analog to interacting bosons in a condensate [3–11]. The external magnetic field acts as a chemical potential in the limit of weak interdimer interactions [12,13]. In real space, the BEC corresponds to a transition to an antiferromagnetic state with staggered magnetization.

This phenomenon has been observed, for example, in prototype systems, such as $BaCuSi_2O_6$ [14] and $TlCuCl_3$ [13]. However, in the case of exchange disorder, the nature of the ground state in a magnetic field and the critical behavior of the field-induced magnetic ordering are not sufficiently understood. Disorder can be induced in such systems, for example, by partial chemical substitution. The most prominent effect of such a chemically induced modification is a shift in the BEC phase boundary in the magnetic phase diagram [2]. However, experiments on nonmagnetically substituted $Ba_3(Cr_{1-x}V_x)O_8$ suggest no significant change in the strength of the intradimer coupling J_0 and an increase in the effective interdimer coupling J_e along with impurity substitution [15]. Similar conclusions have been drawn for $Sr_3Cr_{2-x}M_xO_8$ where Cr was substituted by $M = (V,Mn)$ [16]. Neither any strong suppression of the spin gap nor any signature of a change in the ordered magnetic state was observed up to a 10% substitution level.

By introducing chemical disorder we may create a different critical behavior from the standard BEC one, namely, the critical behavior of a Bose-glass phase [17]. Investigations of possible Bose-glass-related transitions are very interesting although quite challenging. Such a transition was investigated in $Tl_{1-x}K_xCuCl_3$ where a triplon localization in the doped system was observed [18]. Other doped system Br-doped $Ni(Cl_{1-x}Ba_x)_2 - 4SC(NH_2)_2$ studies by nuclear magnetic resonance show a Bose-glass regime where impurity states are localized strongly [19]. This system can be described effectively by two-level impurity states whose pairwise interaction is finite although experimentally suppressed with distance. The doped system $Ba_{3-x}Sr_xCr_2O_8$ to be discussed here represents another promising candidate for the observation of Bose-glass physics [2].

Recently, we reported a peculiar nonlinear tuning of the magnetic intradimer interaction constant J_0 in a corresponding solid solution $Ba_{3-x}Sr_xCr_2O_8$ by varying the Ba and Sr contents [20] as indirectly inferred from magnetization measurements on polycrystalline samples. Here, we report corresponding information about respective data taken on single-crystalline $Ba_{3-x}Sr_xCr_2O_8$ samples and J_0 being directly measured, e.g., by inelastic neutron-scattering techniques.

Here, we report on the growth of $Ba_{3-x}Sr_xCr_2O_8$ single crystals with $x = 2.9$ (3.33% mixing) and $x = 2.8$ (6.66% mixing) and the influence of chemical disorder on the magnetic and the structural properties. Moreover, we have performed inelastic neutron-scattering measurements on single-crystalline $Ba_{3-x}Sr_xCr_2O_8$ with $x = 2.9$ which show three excitation modes, corresponding to three twinned domains that confirm a monoclinic distortion. The hexagonal notation is kept throughout the article. The interaction constants were determined from a random-phase-approximation (RPA) model, and the results are compared to those of $Sr_3Cr_2O_8$ and $Ba_3Cr_2O_8$, respectively.

II. EXPERIMENTAL DETAILS AND CRYSTAL GROWTH

The crystal structure of $Ba_3Cr_2O_8$ presented in Fig. 1 is hexagonal with space-group $R\bar{3}m$ at room temperature. The nuclear structure of the solid solution $Ba_{3-x}Sr_xCr_2O_8$ series has been shown to remain unchanged, but the cell parameters are linearly decreasing with an increase in the Sr content x [21,22]. Single crystals of the unsubstituted end-members $Sr_3Cr_2O_8$ ($x = 3$) and $Ba_3Cr_2O_8$ ($x = 0$) can be grown using the traveling solvent floating-zone method [3,5].

In order to grow $Ba_{3-x}Sr_xCr_2O_8$ crystals, high-purity powders of $SrCO_3$ (Sigma-Aldrich 99.9% purity), $BaCO_3$ (Sigma-Aldrich 99.98% purity), and Cr_2O_8 (Sigma-Aldrich 99.9% purity) were used as starting materials. Several samples were prepared with various Sr content x's using a solid-state reaction: $(3-x)BaCO_3 + xSrCO_3 + Cr_2O_8 \rightarrow Ba_{3-x}Sr_xCr_2O_8 + 3CO_2$. The powders were ground in a planetary ball mill (Pulverisette 5) and heated to 1250 °C for 24 h and quenched in liquid nitrogen to avoid a reaction with atmospheric oxygen and avert impurity phases. This process was repeated three times, and the resulting powders were kept in vacuum. The synthesized powders were examined by powder x-ray diffraction at room temperature and found to be phase pure with the correct hexagonal crystal symmetry $R\bar{3}m$. The powders then were pressed at 2000 bars into cylindrical pellets. The single crystals were grown in the Crystal Laboratory at the Helmholtz Zentrum Berlin für Materialien und Energie (HZB) by using a high-temperature optical floating-zone furnace (Crystal Systems, Inc. Model FZ-T-10000-H-VI-VPO) that was equipped with 300-W halogen lamps as a heat source and four ellipsoidal mirrors thus achieving temperatures up to 2000 °C. Powder x-ray- and Laue-diffraction measurements were performed to check the structure of the powders, crystal purity, and orientation. The relation between Sr and Ba contents was verified by energy-dispersive x-ray (EDX) analysis at various points on the surface and on slices of the crystals in order to check for the crystal homogeneity.

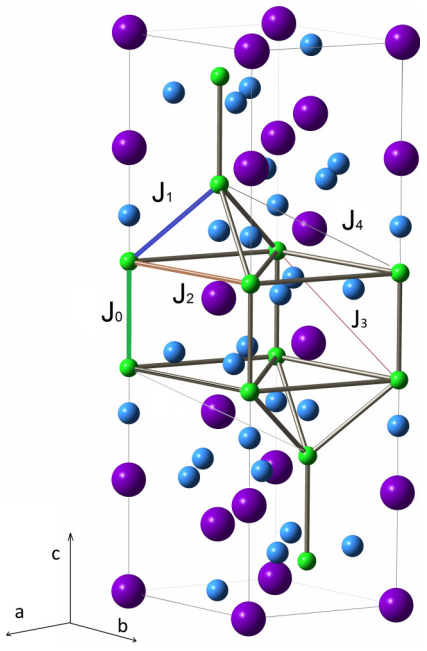

FIG. 1. Crystal structure of $Ba_{3-x}Sr_xCr_2O_8$ at room temperature. The small green circles represent Cr ions, the medium light blue circles are oxygen atoms, and the large violet circles stand for Sr or Ba ions

Commonly, $Ba_3Cr_2O_8$ crystals are grown under argon atmosphere at a relatively high rate [3], whereas $Sr_3Cr_2O_8$ single crystals are grown in flowing synthetic air [5]. $Sr_3Cr_2O_8$ is stable at 1250 °C under a pure oxygen atmosphere. However, a transition of $Sr_3Cr_2O_8$ taking place around 775 °C makes the single-crystal growth challenging due to a chemical reaction with oxygen that changes the oxidation state and phase. Oxidized $Sr_3Cr_2O_8$ is no longer stable in a 1-atm oxygen atmosphere [4]. Moreover, $Sr_3Cr_2O_8$ starts to react strongly with moisture and oxygen and can decompose into $SrCrO_4$ and $Sr_{10}Cr_6O_{24}(OH)_2$ [23].

We examined several preparation conditions for a successful crystal growth. We obtain a stable $Ba_{0.1}Sr_{2.9}Cr_2O_8$ single crystal by using the conditions similar to the preparation of $Sr_3Cr_2O_8$ crystals. However, with a subsequent increase in the Ba content x, the crystal growth becomes unstable, and the crystals tend to break after some time, which might be due to a chemical reaction upon cooling. The crystals of $Ba_{0.2}Sr_{2.8}Cr_2O_8$ grown under argon and 10% oxygen in argon often have a rough surface and contain many crystal grains. This must be due to a different compositional phase diagram in the argon atmosphere, and the necessary temperature to obtain a pure phase probably was not reached. Moreover, an argon atmosphere may create oxygen deficiencies in the crystals. For the present experiment, we chose a single crystal immediately after its preparation to minimize the above-mentioned problems.

We used a synthetic air flow (20.5% oxygen in N_2) of 2 l/min at ambient pressure for the $x = 2.9$ sample. The seed and feed rods were counter-rotated at rates of 30 and 8 rpm, respectively, to obtain a homogeneously illuminated region of the sample. The seed rod was moved slowly out of the hot region for slow cooling and recrystallization. The growth rate is one of the conditions that was varied for the $x = 2.8$ sample growth. An increase in the rate leads to crystal instability. Consequently, the growth process is more stable at the lower growth rate of 4–6 mm/h. The crystals were cylindrical rods of 4–6-mm diameter and 50–100-mm length (Fig. 2). The color of the crystals was dark green, indicating a correct oxidation state Cr^{5+}. Additionally, various annealing treatments were used in order to increase the crystals' ductility. The temperature has to be lower than 350 °C or higher than 850 °C [24]. High-temperature annealing, which requires quenching to a temperature lower than 350 °C, leads to immediate destruction of the crystals. Consequently, the crystals were annealed in a vacuum atmosphere of 1.2×10^{-2} mbars at 300 °C for 6 days. Despite these precautions, $Ba_{0.3}Sr_{2.7}Cr_2O_8$ ($x = 2.7$) crystals were not stable. Growth conditions to obtain single crystals for $x < 2.8$ still are not known.

The crystals for $x = 2.9$ and $x = 2.8$ were characterized by magnetization, neutron-diffraction, and inelastic neutron-scattering measurements. Magnetic susceptibility measurements were performed in a magnetic property measurement system (Quantum Design, Inc.) using a superconducting quantum interference device in magnetic fields of 0.01 and

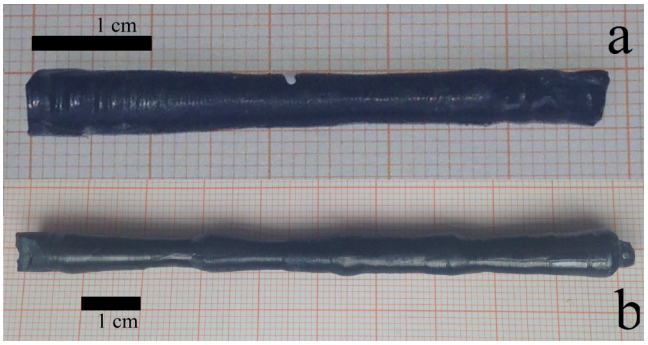

FIG. 2. As-grown samples of $Ba_{3-x}Sr_xCr_2O_8$ (a) $x = 2.9$ and (b) $x = 2.8$. X-ray Laue diffraction on both samples show their crystalline natures as single crystals or multiple crystallites with a shared orientation.

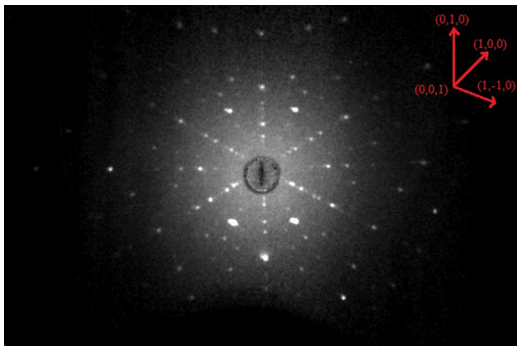

FIG. 3. X-ray Laue pattern of a $Ba_{0.1}Sr_{2.9}Cr_2O_8$ crystal showing the hexagonal symmetry at room temperature.

0.1 T applied perpendicular and parallel to the c axes. The size of the single crystal of $Ba_{0.2}Sr_{2.8}Cr_2O_8$ was not large enough to perform inelastic neutron scattering.

The single-crystal inelastic neutron-scattering measurements were performed on the cold-neutron triple-axis spectrometer (TAS) V-2 FLEXX at HZB on a $Ba_{0.1}Sr_{2.9}Cr_2O_8$ ($x = 2.9$) crystal with a mass of 4 g. The crystal was aligned on the scattering plane $(h,h,l)_h$ and cooled down to 2 K. The measurements were carried out using a vertically and horizontally focusing pyrolytic graphite monochromator and horizontally focusing pyrolytic graphite analyzer along with a beryllium filter. Constant-wave-vector scans were performed to map the dispersion relation in the range up to 7-meV neutron energy transfer with fixed final wave vectors of $k_f = 1.2$ and $k_f = 1.55$ Å^{-1}. The instrumental resolutions with these conditions are 0.098 and 0.192 meV, respectively, as extracted from the FWHM of the vanadium incoherent line.

III. RESULTS AND DISCUSSION

A. Crystal characterization

Powder x-ray-diffraction patterns were taken at room temperature on crushed parts of the crystals before and after annealing. No change in the lattice constants and no impurities were observed. The lattice parameters shrink linearly with decreasing Ba content in accordance with Refs. [21,22]. Interestingly, there is no significant change in the distances between Cr^{5+} ions within a dimer (see Table I).

TABLE I. Intradimer constant J_0, Landé g factors for different crystal orientations, and magnetic impurity content n_p as extracted from dc-magnetic-susceptibility measurements.

	$x = 3$ [6]	$x = 2.9$	$x = 2.8$	$x = 0$ [9]
$g_\perp$	1.98	1.994	1.898	1.99(1)
$g_\parallel$	1.98	2.003	1.959	1.94(1)
J_0 (meV)	5.34	5.04(8)	4.79(7)	2.17(2)
Magnetic impurities n_p	≅0.2%	2.51%	3.25%	≅1%
Cr^{5+}-Cr^{5+} distance (Å) [22]	≅3.755	≅3.77	≅3.79	≅3.96

Both crystals were aligned using Laue-diffraction techniques and cut along the normal plane to the main crystal axes (Fig. 3). EDX analysis was used to estimate the ratio of Sr-to-Ba content. This value is homogeneous along the crystals and agrees well with the expected values (e.g., mixing of Ba concentration ≅3.5% vs the expected value of ≅3.33%) except on the surfaces of the crystals where the Ba ions tend to concentrate. Despite many advantages, the floating-zone method has a number of limitations, e.g., phase separation and incongruent melting. The first limitation can be excluded here because x-ray data show no additional phases present in the crystals. However, the physics of incongruent melting is complex because it is governed by different processes, such as thermal diffusion, partial melting, and segregation. An incongruent melting behavior of $Ba_{3-x}Sr_xCr_2O_8$ could result in a preferred evaporation of Ba in the center of the melt and its migration to the crystal edges.

B. Magnetic susceptibility

In pure systems, spin dimerization is known to occur below 38 K in $Sr_3Cr_2O_8$ [6] and 16 K in $Ba_3Cr_2O_8$ [8], respectively. This manifests itself in a temperature-dependent magnetic susceptibility having a broad maximum and a drop at low temperatures, which is characteristic for systems with nonmagnetic spin-singlet ground states.

The magnetic behavior of the solid-solution compounds is also typical for dimerized spin systems for all other values of x with an interaction constant J_0 that depends strongly on the composition [22]. The magnetic susceptibility measurements for $x = 2.9$ and $x = 2.8$ single crystals in a 0.1-T magnetic field applied perpendicular and parallel, respectively, to the c axes are depicted in Fig. 4. The results are in agreement with previous measurements on polycrystalline samples [22] and with those for $Sr_3Cr_2O_8$ single crystals [6,8,11]. The marked increase in the magnetic susceptibility at very low temperatures suggests the presence of a fraction of paramagnetic impurities (≅3%, see Table I). Our experimental data can be well described with the Bleaney-Bowers formula [Eq. (1)] for interacting spin-$\frac{1}{2}$ dimers with an intradimer exchange constant J_0 and an interdimer coupling constant J_e,

$$M_d(T) = \frac{n_d g^2 \mu_B^2 B_{ext}}{J_e + k_B T(3 + e^{J_0/k_B T})}, \quad (1)$$

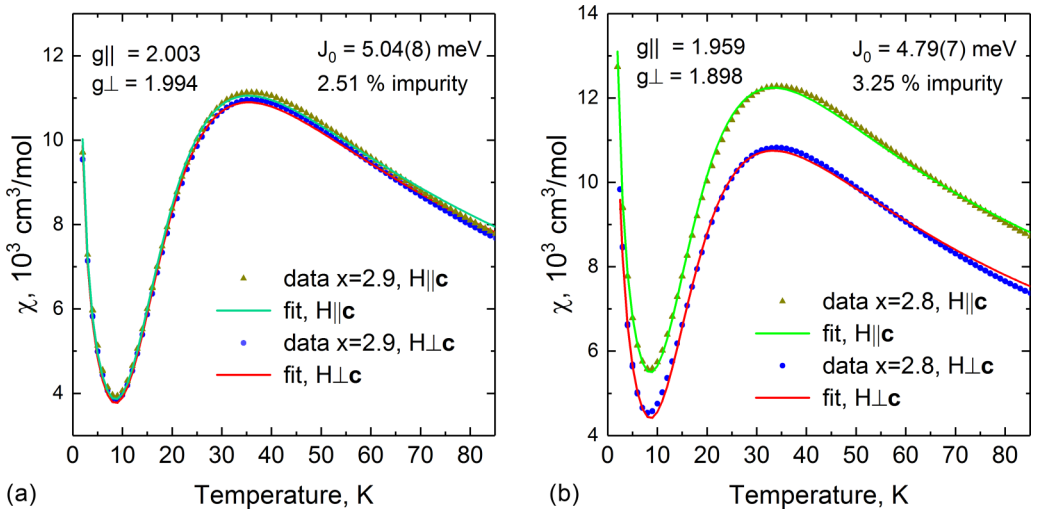

FIG. 4. Magnetic susceptibility data for single crystals of (a) $Ba_{0.1}Sr_{2.9}Cr_2O_8$ and (b) $Ba_{0.2}Sr_{2.8}Cr_2O_8$ with the field perpendicular and parallel, respectively, to c_h.

where n_d is the density of the dimers and g is the Landé g factor. The paramagnetic background can be accounted for with

$$M_p(T) = n_p g \mu_B \frac{1}{2}\left[2\coth\left(\frac{g\mu_B B_{ext}}{k_B T}\right) - \coth\left(\frac{g\mu_B B_{ext}}{2k_B T}\right)\right] \cong n_p \frac{g^2}{4}\frac{\mu_B^2 B_{ext}}{k_B T}, \quad (2)$$

where n_p is the density of the corresponding uncoupled spin-$\frac{1}{2}$ ions. The sum of the above terms with $2n_d + n_p = \text{const}$ fits the experimental data very well (see Fig. 4), but extracting the interdimer interaction constant J_e is problematic as the fit is not very sensitive to variations of J_e. This is also the case for $Sr_3Cr_2O_8$ [11]. The fitted intradimer interaction constants J_0 for our single-crystal samples are presented in Table I together with the g factors for the different crystal orientations and magnetic impurity contents. The values for the parent compounds also have been listed for comparison. As expected and in agreement with our previous results on polycrystalline samples [22], J_0 depends nonlinearly on the stoichiometry and decreases from $x = 3$ to $x = 2.9$ and $x = 2.8$. The magnetic impurity content increases with increasing Ba content, i.e., consequently, decreasing Sr content x. It may stem from impurities undetected by x rays or more likely be due to intrinsic unpaired moments in the disordered crystals.

C. Magnetic excitations

Single-crystal inelastic neutron measurements were performed on the cold-neutron TAS V2-FLEXX at 2 K. The dispersion relation spectrum was mapped at a constant wave vector by scanning the neutron energy, and one of these energy scans is shown in the inset of Fig. 5. In order to map out the dispersion of the singlet-to-triplet excitations, the scans were fitted to the pseudo-Voigt profile, a linear combination of a Gaussian curve and a Lorentzian curve.

Figure 5 shows three modes in the dispersion. The three lines represent the three twins. These modes merge in the center of the hexagonal Brillouin zone (Γ point).

We have fitted the lines with a RPA model where the dispersion relation is defined as

$$\hbar\omega \cong \sqrt{J_0^2 + J_0\gamma(Q)}, \quad (3)$$

with $\gamma(Q)$ as the Fourier sum of the interdimer interactions as described in Refs. [10,11],

$$\gamma(Q) = \sum_i J(R_i)e^{-iQR_i}. \quad (4)$$

As indicated in Fig. 1, the dimers (coupled Cr ions) aligned along the c axis are characterized by the intradimer interaction constant J_0 which is of antiferromagnetic character ($J_0 > 0$). Interdimer interactions are intralayer and interlayer exchange constants and are represented by the interaction constant J_1 with three nearest neighbors in the adjacent layer, J_2 with six next neighbors in plane, J_3 with six next further neighbors on the adjacent plane, and J_4 with three furthest neighbors in the adjacent layer. In our experiment and model, it is not possible to distinguish between J_2 and J_3, only the difference $J_2 - J_3$ can be measured. The intradimer interaction constant J_0 clearly is dominant. In our case we found that J_4 is negligible and it is not taken into account further. The low-temperature structure is monoclinic with three twins which are rotated by 60° with respect to each other and the interactions J_1, J_2, and J_3 become inequivalent. The interaction J_1 then splits in three interactions J_1', J_1'' and J_1''', J_2 (together with J_3) in two J_2''s, two J_2'''s, and two J_2''''s. The value of the effective interdimer interactions is $J_e = |J_1'| + |J_1''| + |J_1'''| + 2(|J_2' - J_3'|) + 2(|J_2'' - J_3''|) + 2(|J_2''' - J_3'''|)$ [11].

The resulting dispersion relation for the three monoclinic twins is illustrated in Fig. 5 where a comparison with the calculated dispersion relations for $x = 2.9$, $x = 3$, and $x = 0$ also is shown. From the six values J_1', $J_{2\text{-}3}' = J_2' - J_3'$ (and the corresponding " ″ " and " ‴ " constants) for *twin* 1, the related constants for the other twins can be found. The physical meaning of these interaction constants is described in detail in Ref. [11]. Our results are presented in Table II along with the corresponding exchange constants for $Sr_3Cr_2O_8$ ($x = 3$) and $Ba_3Cr_2O_8$ ($x = 0$) from the literature [10,11]. The basic

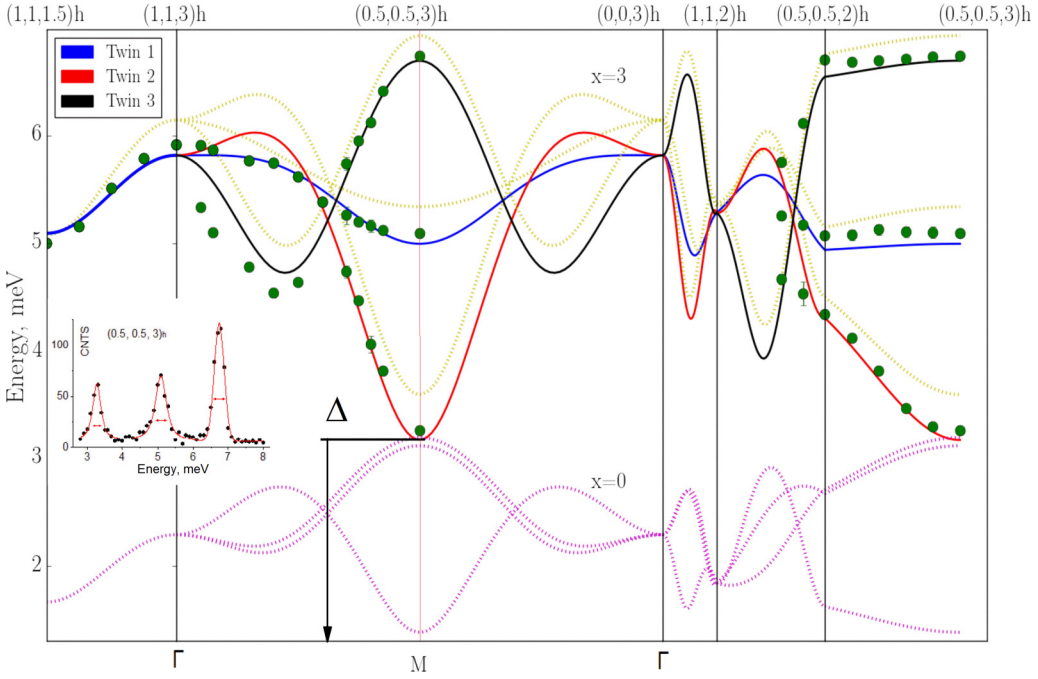

FIG. 5. Dispersion relation for $Ba_{0.1}Sr_{2.9}Cr_2O_8$ for the three monoclinic twins. The green points are the extracted peak positions from the energy scans. The dispersion relation for the $x = 3$ [11] and $x = 0$ [10] compounds within the RPA model are represented by yellow and violet dotted lines, respectively. The resulting RPA model parameters are listed in Table II. A single scan is shown in the inset. The horizontal lines represent the calculated instrument resolution (FWHM).

magnetic structure does not change, but it should be noted that $J'_{2\text{-}3}$ and $J'''_{2\text{-}3}$ have different signs in $Ba_3Cr_2O_8$, which indicates a tendency to ferromagnetic couplings for compounds closer to $Sr_3Cr_2O_8$. The influence of disorder on the structural phase transition along with the linear change in lattice parameters were analyzed previously on polycrystalline $Ba_{3-x}Sr_xCr_2O_8$ samples with varying stoichiometry [21]. Interestingly, the intradimer interaction constant calculated from the neutron powder-diffraction data was reported to change nonlinearly with Sr content x. The peculiar behavior of J_0 can be explained by the changes in the average crystal structure. This result is commensurate with previously extracted values of J_0 from magnetization measurements [22]. The Jahn-Teller distortion induces an orbital ordering [7] and increases the intradimer interaction constant J_0 but seems to gradually be suppressed for intermediate values of x. A larger value of J_0 is accompanied by a stronger symmetry breaking, in other words, by increasing disorder in the system. The tuning of J_0 with varying x therefore allows direct control of the critical magnetic-fields H_c in $Ba_{3-x}Sr_xCr_2O_8$ [20].

TABLE II. Characteristic parameters for the structural transition, triplon condensation, and exchange constants of $Ba_{0.1}Sr_{2.9}Cr_2O_8$ ($x = 2.9$) as compared to corresponding values for $Sr_3Cr_2O_8$ ($x = 3$) and $Ba_3Cr_2O_8$ ($x = 0$).

	$x = 3$ [11]	$x = 2.9$	$x = 0$ [10]
Structural transition			
T_{JT}	285 K	260 K	70 K
Exchange constants (meV)			
J_0	5.551(9)	5.332(2)	2.38
J'_1	−0.04(1)	−0.07(9)	−0.15
J''_1	0.24(1)	0.20(3)	0.08
J'''_1	0.25(1)	0.24(5)	0.10
$(J'_2 - J'_3)$	0.751(9)	0.777(5)	0.10
$(J''_2 - J''_3)$	−0.543(9)	−0.528(1)	−0.52
$(J'''_2 - J'''_3)$	−0.120(9)	−0.112(1)	0.07
J'_4	0.10(2)	0	0.10
J''_4	−0.05(1)	0	0.04
J'''_4	0.04(1)	0	0.09
J_e	3.6(1)	3.36(2)	1.94
J_e/J_0	0.64(2)	0.63(1)	0.8151
Triplon condensation			
$\mu_0 H_{c1}$	30.4 T	28.8 T	12.5 T

The smaller lattice distances in $Sr_3Cr_2O_8$ than in $Ba_3Cr_2O_8$ lead to a larger intradimer interaction constant and spin gap. The values of the intradimer interaction constants J_0 are smaller for $Ba_3Cr_2O_8$ (2.38 meV) and $Ba_{0.1}Sr_{2.9}Cr_2O_8$ [5.332(2) meV] when compared with $Sr_3Cr_2O_8$ [5.551(9) meV]. This can be explained easily by the comparably shorter atomic distances in $Sr_3Cr_2O_8$. The Dzyaloshinsky-Moriya anisotropy term also should play an important role on the not-equal exchange interactions found [25,26]. The ratio of the excitation bandwidth J_e to the average mode energy J_e/J_0 is larger in $Sr_3Cr_2O_8$ [0.64(2) meV] than for $Ba_{0.1}Sr_{2.9}Cr_2O_8$ [0.63(1) meV] and smaller than for $Ba_3Cr_2O_8$ (0.8151 meV). The resulting spin gap in $Sr_3Cr_2O_8$ [3.451(8) meV] is larger than in $Ba_{0.1}Sr_{2.9}Cr_2O_8$ (3.174 meV) and $Ba_3Cr_2O_8$ (1.38 meV). We therefore can expect that the critical magnetic field where the spin gap closes (i.e., the onset of the BEC) is smaller in $Ba_{0.1}Sr_{2.9}Cr_2O_8$ than in $Sr_3Cr_2O_8$ by roughly 8%. From high-field magnetization measurements on polycrystalline samples

at $T = 1.5$ K [20], we indeed inferred a $\mu_0 H_{c1} \cong 28.8$ T for $Ba_{0.1}Sr_{2.9}Cr_2O_8$ as compared to 30.4 T in $Sr_3Cr_2O_8$.

The inset in Fig. 5 shows one of the multiple TAS scans at $(0.5,0.5,3)_h$. The three peaks are only slightly broader than the instrumental resolution, indicating long-range exitations. Scans also were extended below the gap energy down to 1.7 meV, but no in-gap intensity was found. These two characteristics show that there is no considerable magnetic disorder caused by the random substitution of Sr by Ba.

The value of the intradimer interaction constant for $x = 2.9$ (5.04 meV) as obtained by magnetization measurements is somewhat lower than that from fitting the inelastic neutron-scattering data to a RPA model (5.332 meV). This may reflect a general trend as J_0 values reported for $x = 3$ ($Sr_3Cr_2O_8$) from magnetic susceptibility data vary from 5.34 meV [6] and 5.30 meV [9] to 5.51 meV [11], whereas ion neutralization spectroscopy (INS) data yield a larger value of $J_0 = 5.55$ meV [11]. A similar feature also has been observed in corresponding data for $x = 0$ ($Ba_3Cr_2O_8$) with $J_0 \cong 2.17(2)$ meV (magnetization) and 2.38 meV (INS), respectively [9]. We believe that a comparison of such data within the same measurement technique (i.e., within Tables I and II) yields the correct trend, whereas the true values of J_0 may be closer to those obtained by inelastic neutron-scattering data. However, both the RPA and the Bleaney-Bowers approximation are mean-field approximations to the multibody phenomena. INS gives more precise values for J_e because corresponding fits are performed for larger data sets involving several directions in reciprocal space.

IV. CONCLUSIONS

The conditions to grow single crystals of $Ba_{0.1}Sr_{2.9}Cr_2O_8$ and $Ba_{0.2}Sr_{2.8}Cr_2O_8$ by the floating-zone method were examined, and their structural and magnetic properties were explored. The magnetic susceptibilities for different field orientations indicate a certain anisotropy of the Landé g factor for magnetic fields parallel or perpendicular, respectively, to the c_h axes, which is larger in $Ba_{0.2}Sr_{2.8}Cr_2O_8$ than in $Ba_{0.1}Sr_{2.9}Cr_2O_8$. Inelastic neutron-scattering measurements of $Ba_{0.1}Sr_{2.9}Cr_2O_8$ confirm a change in the magnetic interaction constants and the spin gap upon a partial substitution of Sr by Ba. The observed dispersion relation is reproduced excellently by the RPA model. No sign of magnetic disorder is detected, neither in the form of the appearance of in-gap intensity nor as a noticeable energy broadening of the excitations. The intradimer interaction J_0 decreases for $x = 2.9$ by about 4% as compared to $x = 3$ when chemical disorder is introduced, whereas the effective interdimer interaction decreases by about 7%, and the spin gap is reduced by about 8%. However, the $x = 2.9$ compound does not show any magnetic disorder. Higher substitution levels in this family of compounds may provide a playground to study disorder effects in mixed spin-dimer systems. Unfortunately, the inelastic neutron-scattering experiment failed on the $Ba_{0.2}Sr_{2.8}Cr_2O_8$ crystal due to instability, which led to a decrease in crystal size, making these experiments impossible. Further investigations on the nuclear crystal structure are underway and will be provided in a separate paper.

ACKNOWLEDGMENTS

We thank B. Lake for the possibility to realize this research, A. T. M. Nazmul Islam for the help with crystal growth, and the Helmholz Zentrum Berlin for the access to neutron beam time at the research reactor BER II. We thank E. Pomjakushina for the EDX analysis. This work was supported by the Swiss National Science Foundation Grant No. 21-153659.

[1] V. Zapf, M. Jaime, and C. D. Batista, Rev. Mod. Phys. **86**, 563 (2014).
[2] A. Zheludev and T. Roscilde, C. R. Phys. **14**, 740 (2013).
[3] A. A. Aczel, D. L. Quintero-Castro, B. Lake, K. Siemensmeyer, K. Kiefer, Y. Skourski, and T. Herrmannsdorfer, Cryst. Growth Des. **10**, 465 (2010).
[4] K. T. Jacob and K. P. Abraham, J. Phase Equilib. **21**, 46 (2000).
[5] A. T. M. Nazmul Islam, H. A. Dabkowska, P. R. Provencher, and G. M. Luke, J. Cryst. Growth **310**, 870 (2008).
[6] Y. Singh and D. C. Johnston, Phys. Rev. B **76**, 012407 (2007).
[7] L. C. Chapon, C. Stock, P. G. Radaelli, and C. Martin, arXiv:0807.0877.
[8] A. A. Aczel, Y. Kohama, C. Marcenat, F. Weickert, M. Jaime, O. E. Ayala-Valenzuela, R. D. McDonald, S. D. Selesnic, H. A. Dabkowska, and G. M. Luke, Phys. Rev. Lett. **103**, 207203 (2009).
[9] A. A. Aczel, Y. Kohama, M. Jaime, K. Ninios, H. B. Chan, L. Balicas, H. A. Dabkowska, and G. M. Luke, Phys. Rev. B **79**, 100409(R) (2009).
[10] M. Kofu, H. Ueda, H. Nojiri, Y. Oshima, T. Zenmoto, K. C. Rule, S. Gerischer, B. Lake, C. D. Batista, Y. Ueda, and S.-H. Lee, Phys. Rev. Lett. **102**, 177204 (2009).
[11] D. L. Quintero-Castro, B. Lake, E. M. Wheeler, A. T. M. N. Islam, T. Guidi, K. C. Rule, Z. Izaola, M. Russina, K. Kiefer, Y. Skourski, and T. Herrmannsdorfer, Phys. Rev. B **81**, 014415 (2010).
[12] T. Giamarchi, C. Ruegg, and O. Tchernyshyov, Nat. Phys. **4**, 198 (2008).
[13] T. Nikuni, M. Oshikawa, A. Oosawa, and H. Tanaka, Phys. Rev. Lett. **84**, 5868 (2000).
[14] M. Jaime, V. F. Correa, N. Harrison, C. D. Batista, N. Kawashima, Y. Kazuma, G. A. Jorge, R. Stern, I. Heinmaa, S. A. Zvyagin, Y. Sasago, and K. Uchinokura, Phys. Rev. Lett. **93**, 087203 (2004).
[15] T. Hong, L. Y. Zhu, X. Ke, V. O. Garlea, Y. Qiu, Y. Nambu, H. Yoshizawa, M. Zhu, G. E. Granroth, A. T. Savici, Z. Gai, and H. D. Zhou, Phys. Rev. B **87**, 144427 (2013).
[16] S. Chattopadhyay, S. Giri, and S. Majumdar, Eur. Phys. J. B **85**, 4 (2012).
[17] M. P. A. Fisher, P. B. Weichman, G. Grinstein, and D. S. Fisher, Phys. Rev. B **40**, 546 (1989).
[18] F. Yamada, H. Tanaka, T. Ono, and H. Nojiri, Phys. Rev. B **83**, 020409(R) (2011).
[19] A. Orlova, R. Blinder, E. Kermarrec, M. Dupont, N. Laflorencie, S. Capponi, H. Mayaffre, C. Berthier, A. Paduan-Filho, and M. Horvatic, Phys. Rev. Lett. **118**, 067203 (2017).

[20] H. Grundmann, A. Gazizulina, A. Schilling, F. von Rohr, T. Forster, and L. Peters, New J. Phys. **18**, 033001 (2016).
[21] H. Grundmann, A. Schilling, M. Medarde, and D. Sheptyakov, Phys. Rev. B **90**, 075101 (2014).
[22] H. Grundmann, A. Schilling, C. A. Marjerrison, H. A. Dabkowska, and B. D. Gaulin, Mater. Res. Bull **48**, 3108 (2013).
[23] Y. K. Kisil, N. G. Sharova, and B. V. Slobodin, Inorg. Mater. **25**, 1490 (1989).
[24] American Ceramics Society database.
[25] Z. Wang, D. Kamenskyi, O. Cepas, M. Schmidt, D. L. Quintero-Castro, A. T. M. N. Islam, B. Lake, A. A. Aczel, H. A. Dabkowska, A. B. Dabkowski, G. M. Luke, Yuan Wan, A. Loidl, M. Ozerov, J. Wosnitza, S. A. Zvyagin, and J. Deisenhofer, Phys. Rev. B **89**, 174406 (2014).
[26] T. Dodds, B.-J. Yang, and Y. B. Kim, Phys. Rev. B **81**, 054412 (2010).